Exponential Growth of Nonlinear Ballooning Instability

P. Zhu, C. C. Hegna, and C. R. Sovinec
Center for Plasma Theory and Computation
University of Wisconsin-Madison
Madison, WI 53706, USA

Abstract

Recent ideal magnetohydrodynamic (MHD) theory predicts that a perturbation evolving from a linear ballooning instability will continue to grow exponentially at the same linear growth rate globally in the intermediate nonlinear phase. This theoretical prediction is confirmed in direct MHD simulations of nonlinear ballooning instability growth in a tokamak. The Lagrangian compression, which serves as a measure of nonlinearity of the ballooning perturbation, is monitored in the simulation. When the Lagrangian compression becomes of order of unity, the instability enters the intermediate nonlinear phase. During this phase, the maximum plasma displacement amplitude as well as the total kinetic energy continues to grow exponentially at the rate corresponding to the linear phase, despite the nonlinear amplitude of the perturbation.

The ballooning instability is a pressure gradient driven mode in magnetized plasma that is localized in the unfavorable curvature regions of magnetic field lines [1–3]. The ballooning instability is a ubiquitous, fundamental process [4–6] that is involved in many phenomena in natural and laboratory magnetized plasmas with high β values. Here β is the ratio of plasma and magnetic pressures. Relative to other MHD instabilities (e.g. [7, 8]), the nonlinear behavior of ballooning instability is less well understood. There is renewed interest in nonlinear ballooning due to its possible roles in edge localized modes (ELMs) in tokamaks [9–11] and the substorm onset process in the Earth's magnetotail [12–14]. Early reduced MHD simulations of high-β tokamak plasmas indicate the formation of a singular current sheet in the final nonlinear state of a ballooning instability which had evolved from a linear mode with very low toroidal mode number n ($n = 1$) [15]. More recently, 3D resistive MHD simulations of nonlinear ballooning instability were applied to model high-β disruptions in tokamaks [16, 17]. Analytical theory has been developed for nonlinear ballooning growth of a marginally unstable configuration in the early nonlinear regime [18–20]. Analytical theory of the intermediate nonlinear regime of ballooning instability has been developed lately to better understand simulations and experiments [21–23].

The onset of ELMs in experiment is well predicted by the breaching of linear ideal MHD ballooning instability boundaries [11]. Filamentary structures and their localization in the unfavorable curvature region of the tokamak edge have been routinely observed during periods of ELMs in recent Mega Amp Spherical Tokamak (MAST) experiments [24, 25] as well as in two-fluid and extended MHD simulations [26, 27]. This suggests that the ballooning instability properties of the pedestal region continue to play a dominant role in determining the nonlinear temporal and spatial structures of ELMs. Thus, it may be possible to understand the dynamics of the ELM filaments in terms of the nonlinear properties of the ballooning instability.

Different phases of ELM evolution may relate to different linear and nonlinear regimes of ballooning instability. To describe the different nonlinear phases, we introduce two small parameters given by

$$n^{-1} = \frac{k_\parallel}{k_\perp} \ll 1, \qquad \varepsilon = \frac{|\boldsymbol{\xi}|}{L_{\rm eq}} \ll 1. \tag{1}$$

Here, $k_\parallel$ and $k_\perp$ are the dominant wavenumbers of the perturbation parallel to and perpendicular to the equilibrium magnetic field, respectively; $\boldsymbol{\xi}$ is the plasma displacement produced by instability, and $L_{\rm eq}$ is the equilibrium scale length (which is used as the normalization

length later so that $L_{\rm eq} = 1$).

The linear structure and growth rates of ballooning instabilities can be determined using an asymptotic expansion of the linearized ideal MHD equation in terms of n^{-1} [2, 3, 28]. The mode structure in the fastest varying direction perpendicular to the magnetic field is given by n^{-1}, which is the scale of the dominant wavelength. At lowest order in n^{-1}, the ballooning mode is described by two coupled one-dimensional ordinary differential equations along each field line, which together with proper boundary conditions, determines the local eigenfrequency or local growth rate as well as the local mode structure along the equilibrium magnetic field as a function of magnetic flux surface, field line, and radial wavenumber. At higher order in n^{-1}, a global eigenmode equation, the envelope equation, which uses information from the local mode calculations, governs the global growth rate and mode structure across magnetic surfaces. In axisymmetric equilibria, the global growth rate is given by the most unstable value of the local growth rate with stabilizing corrections of order n^{-1}. As shown earlier [18–22] and in this work, the properties of linear ballooning instability are crucial to the construction and understanding of the theory of nonlinear ballooning instability.

The perturbation amplitude of the nonlinear ballooning mode, measured by ε ($\sim |\boldsymbol{\xi}|$), can be compared to the characteristic spatial scales of its linear mode structure. In the early nonlinear regime, the filament scale $|\boldsymbol{\xi}|$ across the magnetic flux surface is comparable to the mode width λ_α in the most rapidly oscillating direction, $|\boldsymbol{\xi}| \sim \lambda_\alpha \sim n^{-1}$ [18–20]. In this regime, the nonlinear convection across the flux surface is small relative to the mode width λ_Ψ in that direction. The dominant effect of the nonlinearities is to modify the radial envelope equation describing mode evolution across the magnetic surface. Here Ψ and α are the flux and field line labels, respectively, which are later used to define the equilibrium magnetic field in Eq. (4). As the mode continues to grow, it enters the intermediate nonlinear regime, in which $|\boldsymbol{\xi}| \sim \lambda_\Psi \sim n^{-1/2}$; the plasma displacement across the magnetic flux surface becomes of the same order as the mode width in the same direction [21, 22]. In this regime, effects due to convection and compression are no longer small. Nonlinearities due to convection and compression, together with nonlinear line-bending forces, directly modify the "local" mode evolution along the magnetic field line. In the late nonlinear regime, the ballooning filament growth may exceed the scale of the pedestal width. Eventually, these ballooning filaments could detach from edge plasma and propagate into the scrape-off-layer region, as indicated

from recent experiment [25]. In this work, we consider the physics of the intermediate nonlinear phase and leave discussion of the late nonlinear regime for subsequent work.

It is conceivable that the linear to early nonlinear regime of the ballooning instability of the pedestal may correspond to the precursor phase of ELMs since the onset of the ELMs have been consistently correlated to the breaching of the linear stability boundary of the peeling-ballooning modes [9, 11]. Earlier theory attempted to explain the collapse onset phase of ELMs by invoking a finite time-like singularity associated with the early nonlinear ballooning instability of a marginally unstable configuration ("Cowley-Artun" regime) [18–20]. Such a scenario, however, has yet to be confirmed by direct MHD simulations, probably due to the rather limited range of validity for that regime. In contrast, there is a good agreement between the solutions of the intermediate nonlinear regime equations and results from direct MHD simulations for both the case of a line-tied g-mode [22] and the ballooning instability of a tokamak (as shown in this paper). It is likely that the intermediate nonlinear regime may better characterize the transition from the precursor phase to the collapse onset of an ELM. This regime could become particularly relevant for application to ELMs as the width of the transport barrier (or pedestal) region is comparable to the mode width of the dominant ballooning instability.

In the following the theory of the intermediate nonlinear regime of the ballooning instability is briefly reviewed. A detailed calculation can be found in [23]. We then describe the comparison between the theory prediction and direct MHD simulations of the ballooning instability in a tokamak.

The nonlinear theory of ballooning mode can be conveniently developed in the Lagrangian formulation of the ideal MHD model [29]

$$\begin{aligned}\frac{\rho_0}{J}\nabla_0\mathbf{r}\cdot\frac{\partial^2\boldsymbol{\xi}}{\partial t^2} = &-\nabla_0\left[\frac{p_0}{J^\gamma}+\frac{\left(\mathbf{B}_0\cdot\nabla_0\mathbf{r}\right)^2}{2J^2}\right]\\ &+\nabla_0\mathbf{r}\cdot\left[\frac{\mathbf{B}_0}{J}\cdot\nabla_0\left(\frac{\mathbf{B}_0}{J}\cdot\nabla_0\mathbf{r}\right)\right]\end{aligned} \tag{2}$$

where

$$\mathbf{r}(\mathbf{r}_0,t)=\mathbf{r}_0+\boldsymbol{\xi}(\mathbf{r}_0,t),\quad \nabla_0=\frac{\partial}{\partial\mathbf{r}_0},\quad J(\mathbf{r}_0,t)=|\nabla_0\mathbf{r}|. \tag{3}$$

Here, $\mathbf{r}_0$ denotes the initial location of each plasma element in the equilibrium, $\boldsymbol{\xi}$ is the plasma displacement from the initial location, and $J(\mathbf{r}_0,t)$ is the Jacobian for the Lagrangian transformation from $\mathbf{r}_0$ to $\mathbf{r}(\mathbf{r}_0,t)$; ρ_0, p_0, and $\mathbf{B}_0$ are the equilibrium mass density, pressure,

and magnetic field, respectively. We consider a general magnetic configuration that can be described by

$$\mathbf{B}_0 = \nabla_0\Psi_0 \times \nabla_0\alpha_0 \tag{4}$$

in a nonorthogonal Clebsch coordinate system (Ψ_0, α_0, l_0), where Ψ_0 is the magnetic flux label, α_0 the field line label, and l_0 the measure of field line length. The corresponding coordinate Jacobian is given by $(\nabla_0\Psi_0 \times \nabla_0\alpha_0 \cdot \nabla_0 l_0)^{-1} = |\mathbf{B}_0|^{-1}$.

The intermediate nonlinear regime is defined by the ordering $\varepsilon \sim \mathcal{O}(n^{-1/2})$ [21, 22]. In this regime the plasma displacement $\boldsymbol{\xi}$ can be expanded as a single series in $n^{-1/2}$

$$\boldsymbol{\xi}(\sqrt{n}\Psi_0, n\alpha_0, l_0, t) = \sum_{j=1}^{\infty} n^{-\frac{j}{2}} \left(\mathbf{e}_\perp \xi^{\Psi}_{\frac{j}{2}} + \frac{\mathbf{e}_\wedge}{\sqrt{n}} \xi^{\alpha}_{\frac{j+1}{2}} + \mathbf{B}\xi^{\|}_{\frac{j}{2}} \right) \tag{5}$$

where

$$\mathbf{e}_\perp = \frac{\nabla_0\alpha_0 \times \mathbf{B}}{B^2}, \quad \mathbf{e}_\wedge = \frac{\mathbf{B} \times \nabla_0\Psi_0}{B^2}. \tag{6}$$

Here and subsequently we drop the subscript "0" in the equilibrium MHD fields ρ_0, p_0, and $\mathbf{B}_0$ for convenience. The spatial structure of the perturbation quantities is determined by the conventional ballooning theory ordering; the plasma displacement $\boldsymbol{\xi}$ and the Lagrangian Jacobian J are functions of the normalized coordinates (Ψ, α, l), where $\Psi = \sqrt{n}\Psi_0$, $\alpha = n\alpha_0$, $l = l_0$.

Evolution equations for the ideal MHD plasma displacement in the intermediate nonlinear regime can be obtained using a perturbation theory in $\varepsilon \sim n^{-1/2} \ll 1$. These equations are given by [23]

$$\left[\Psi + \xi^{\Psi}_{\frac{1}{2}}, \rho|\mathbf{e}_\perp|^2 \partial_t^2 \xi^{\Psi}_{\frac{1}{2}} - \mathcal{L}_\perp(\xi^{\Psi}_{\frac{1}{2}}, \xi^{\|}_{\frac{1}{2}}) \right] = 0, \tag{7}$$

$$\rho B^2 \partial_t^2 \xi^{\|}_{\frac{1}{2}} - \mathcal{L}_\|(\xi^{\Psi}_{\frac{1}{2}}, \xi^{\|}_{\frac{1}{2}}) = 0. \tag{8}$$

where $\partial_t = (\partial/\partial t)_{\mathbf{r}_0}$, $[A, B] \equiv \partial_\Psi A \partial_\alpha B - \partial_\alpha A \partial_\Psi B$, $\mathcal{L}_\perp$ ($\mathcal{L}_\|$) is the perpendicular (parallel) component of the local linear ballooning operator [19, 23]. The structure of these two equations indicates that the solution satisfies the following general form

$$\rho|\mathbf{e}_\perp|^2 \partial_t^2 \xi^{\Psi}_{\frac{1}{2}} = \mathcal{L}_\perp(\xi^{\Psi}_{\frac{1}{2}}, \xi^{\|}_{\frac{1}{2}}) + N(\Psi + \xi^{\Psi}_{\frac{1}{2}}, l, t), \tag{9}$$

$$\rho B^2 \partial_t^2 \xi^{\|}_{\frac{1}{2}} = \mathcal{L}_\|(\xi^{\Psi}_{\frac{1}{2}}, \xi^{\|}_{\frac{1}{2}}) \tag{10}$$

where $N(\widetilde{\Psi}, l, t)$ is a function of the distorted flux function

$$\widetilde{\Psi} = \Psi + \xi^{\Psi}_{\frac{1}{2}}, \tag{11}$$

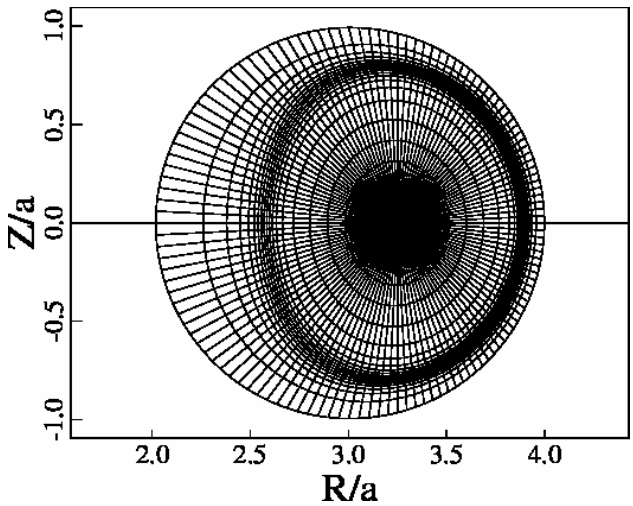

FIG. 1: The finite element mesh based on a tokamak equilibrium generated using the ESC solver. R and Z are the cylindrical coordinates; a is the minor radius. The rings of grid lines approximate contours of constant equilibrium pressure.

field line coordinate l and time. A particular choice is

$$N(\widetilde{\Psi}, l, t) = 0 \tag{12}$$

which implies that solutions of the linear local ballooning mode equations continue to be solutions of the nonlinear ballooning equations (7) and (8) formally. The nonlinear contributions to equations (7) and (8) vanish for any nonlinear solution that assumes the linear ballooning mode structure in Lagrangian coordinates. As a consequence, global quantities of the perturbation, such as the maximum magnitude of plasma displacement and the total kinetic energy, grow exponentially at the growth rate of the linear phase, even in the intermediate nonlinear stage.

This theoretical prediction has been confirmed in recent direct MHD simulations of nonlinear ballooning instability in a tokamak using the NIMROD code [30]. The simulation starts with a small perturbation to a toroidal tokamak equilibrium generated with the ESC solver [31] (Fig. 2). The equilibrium has a circular shaped boundary, with the major radius $R_0 = 3$ and the minor radius $a = 1$ (all quantities are in SI units). The pressure profile is pedestal-like: $\mu_0 p(x) = p_p + h_p \tanh\left[x_p - x)/L_p\right]$, where $p_p = 0.045, h_p = 0.044, x_p = 0.7, L_p = 0.05$, $x = \sqrt{\Psi_T/\Psi_{Ta}}$, and Ψ_T (Ψ_{Ta}) is the toroidal flux (at boundary). The safety factor q is monotonically increasing: $q = q_0[1 + (q_a/q_0 - 1)x^4]$, with $q_0 = 1.05, q_a = 3$. The

magnetic field at magnetic axis is $B_0 = 1$. The initial perturbation is dominated by an $n = 15$ Fourier component in toroidal direction. The perturbation is advanced using the standard set of ideal MHD equations (with resistivity $\eta = 0$) in the NIMROD simulation [30]. We also advance the plasma displacement as an extra field in Eulerian coordinates using

$$\partial_t \boldsymbol{\xi}(\mathbf{r}, t) + \mathbf{u}(\mathbf{r}, t) \cdot \nabla \boldsymbol{\xi}(\mathbf{r}, t) = \mathbf{u}(\mathbf{r}, t) \tag{13}$$

where $\mathbf{u}(\mathbf{r}, t)$ is the velocity field, $\partial_t = (\partial/\partial t)_{\mathbf{r}}$, and $\nabla = \partial/\partial \mathbf{r}$. We then calculate the Lagrangian compression $\nabla_0 \cdot \boldsymbol{\xi}$ from the Eulerian tensor $\nabla \boldsymbol{\xi}$ using the identity

$$\nabla_0 \cdot \boldsymbol{\xi} = \mathrm{Tr}(\nabla_0 \boldsymbol{\xi}) = \mathrm{Tr}[(\mathbf{I} - \nabla \boldsymbol{\xi})^{-1} \cdot \nabla \boldsymbol{\xi}]. \tag{14}$$

Both the maximum plasma displacement $|\boldsymbol{\xi}|_{\max}$ and the maximum Lagrangian compression $(\nabla_0 \cdot \boldsymbol{\xi})_{\max}$ of the entire simulation domain evolve at the same linear growth rate during the phase $10 \lesssim t \lesssim 30$. When the Lagrangian compression $(\nabla_0 \cdot \boldsymbol{\xi})_{\max}$ becomes of order unity, the perturbation has evolved into the intermediate nonlinear phase, which is characterized by the ordering

$$\boldsymbol{\xi} \cdot \nabla_0 \sim \nabla_0 \cdot \boldsymbol{\xi} \sim \lambda_\Psi^{-1} \xi^\Psi + \lambda_\alpha^{-1} \xi^\alpha \sim 1. \tag{15}$$

However, the maximum plasma displacement itself continues to grow exponentially with the same growth rate of the linear phase of the mode well into the intermediate nonlinear phase. This behavior is demonstrated in Fig. 2, which is consistent with the special solution of the analytic theory [23]. The sudden enhanced growth of the Lagrangian compression $\nabla_0 \cdot \boldsymbol{\xi}$ in Fig. 2 above the intermediate nonlinear regime may reflect the fact that the matrix $(\mathbf{I} - \nabla \boldsymbol{\xi})$ could become nearly singular during the nonlinear phase, even though the Eulerian compression $\nabla \cdot \boldsymbol{\xi}$ remains finite. For the case shown in Fig. 2, the tokamak minor radius is $a = 1$, and the pressure pedestal width is $L_{\mathrm{ped}} \sim 0.1$. As the Lagrangian compression $(\nabla_0 \cdot \boldsymbol{\xi})_{\max} >> 1$, the mode traverses the intermediate nonlinear phase, and the maximum plasma displacement $|\boldsymbol{\xi}|_{\max}$ surpasses the pedestal scale length L_{ped}. By then the analytical theory developed in Ref. [23] no longer applies.

In summary, direct MHD simulations have confirmed a prediction from a recently developed ideal MHD theory for the ballooning mode growth in the intermediate nonlinear regime. Both theory and simulations have demonstrated that a perturbation that evolves from a linear ballooning instability will continue to grow exponentially at the same growth rate in global quantities, and maintain the filamentary mode structure of the corresponding

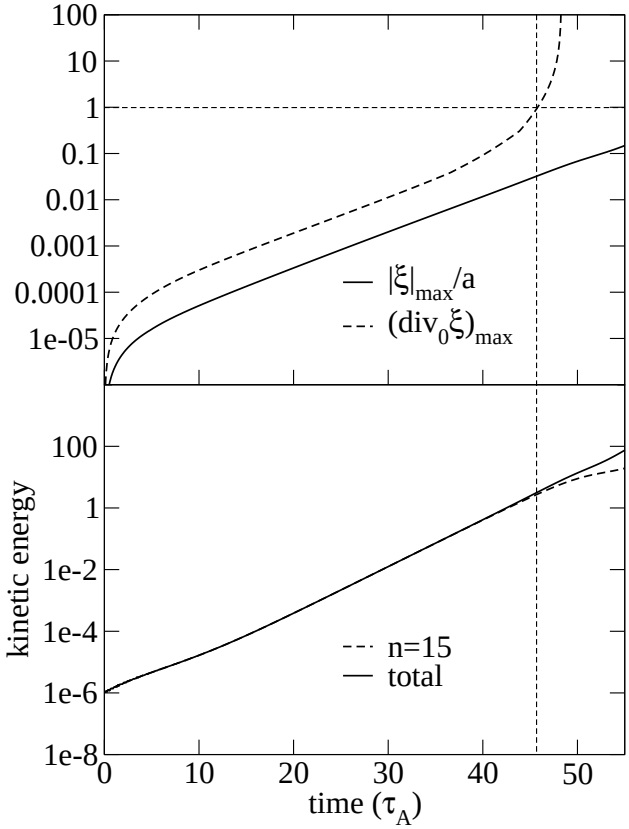

FIG. 2: Top: Growth of the maximum amplitude of plasma displacement $|\boldsymbol{\xi}|_{\max}$ normalized by minor radius a (solid line) and growth of the maximum Lagrangian compression $(\nabla_0 \cdot \boldsymbol{\xi})_{\max}$ (dashed line) calculated from a NIMROD simulation. The time is normalized by the Alfvén time $\tau_{\mathrm{A}} = 1\mu s$. The horizontal and vertical dashed lines mark the intermediate nonlinear regime as determined by the ordering $\nabla_0 \cdot \boldsymbol{\xi} \sim 1$. Bottom: Growth of the total kinetic energy (solid line) and the kinetic energy of the $n = 15$ Fourier component (dashed line). The vertical dashed line marks the intermediate nonlinear regime in time.

linear phase in the intermediate nonlinear stage in the Lagrangian coordinates. This may explain why in experiments, the nonlinear ELM filament strongly resembles the structure of a linear ballooning filament, and linear analyses have often been able to match and predict the observed mode structures of ELMs [11, 26]. The theory prediction and the simulation confirmation for nonlinear ballooning instability are consistent with the agreement observed in previous numerical analysis and simulations of the line-tied g mode [22, 32]. This is because both modes share similar linear and nonlinear dynamics despite the different associated geometry [23]. Due to its simpler geometry, the line-tied g mode has been studied as a

prototype for the more geometrically complicated ballooning instability [18, 21, 22, 32, 33]. The agreement between theory and simulations on nonlinear ballooning instability is a step toward understanding the precursor and onset phases of ELMs.

Our analytical model focuses on the nonlinear growth of the ballooning filament in the ideal MHD regime. The adoption of the ideal MHD model by no means implies the insignificance of other nonideal MHD effects, such as those of two-fluid physics, resistivity, and finite-Larmor-radius (FLR), on ballooning filament dynamics. Rather, this approach allows the systematic isolation, identification, and inclusion of the dominant nonlinear mechanisms in each regime. This study is an important step towards the construction of a more relevant two-fluid MHD model for the dynamics of nonlinear ballooning mode and ELM filaments. The roles of FLR and two-fluid effects on nonlinear ballooning have yet to be fully elucidated and will be the subject of future work.

This research is supported by U.S. Department of Energy under Grants No. DE-FG02-86ER53218 and No. DE-FC02-08ER54975. Computations were performed in National Energy Research Scientific Computing Center, which is supported by U.S. Department of Energy under Contract No. DE-AC03-76SF00098. The authors are grateful for discussions with J. D. Callen, S. C. Cowley, and P. B. Snyder, and for contributions to code development from the NIMROD team. P. Zhu would like to thank A. H. Hammond and S. E. Kruger for the assistance in using the ESC solver.

[1] B. Coppi, *Phys. Rev. Lett.* **39**, 939 (1977).

[2] J. W. Connor, R. J. Hastie, and J. B. Taylor, *Phys. Rev. Lett.* **40**, 396 (1978).

[3] R. L. Dewar and A. H. Glasser, *Phys. Fluids* **26**, 3038 (1983).

[4] E. Hameiri, in *Sherwood Meeting on Theoretical Aspects of Controlled Thermonuclear Research, April 18-20, 1979, Mount Pocono, PA* (1979).

[5] G. O. Spies, *Nucl. Fusion* **19**, 1532 (1979).

[6] E. Hameiri, *Comm. Pure Appl. Math.* **38**, 43 (1985).

[7] P. H. Rutherford, *Phys. Fluids* **16**, 1903 (1973).

[8] M. N. Rosenbluth, R. Y. Dagazian, and P. H. Rutherford, *Phys. Fluids* **16**, 1894 (1973).

[9] C. C. Hegna, J. W. Connor, R. J. Hastie, and H. R. Wilson, *Phys. Plasmas* **3**, 584 (1996).

[10] J. W. Connor, *Plasma Phys. Control. Fusion* **40**, 531 (1998).

[11] P. B. Snyder, H. R. Wilson, J. R. Ferron, L. L. Lao, A. W. Leonard, T. H. Osborne, A. D. Turnbull, D. Mossessian, M. Murakami, and X. Q. Xu, *Phys. Plasmas* **9**, 2037 (2002).

[12] A. Roux, S. Perraut, P. Robert, A. Morane, A. Pedersen, A. Korth, G. Kremser, B.Aparicio, D. Rodgers, and R. Pellinen, *J. Geophys. Res.* **96**, 17697 (1991).

[13] A. Bhattacharjee, Z. W. Ma, and X. Wang, *Geophys. Rev. Lett.* **25**, 861 (1998).

[14] P. Zhu, C. R. Sovinec, C. C. Hegna, A. Bhattacharjee, and K. Germaschewski, *J. Geophys. Res.* **112**, A06222 (2007).

[15] D. A. Monticello, W. Park, S. Jardin, M. S. Chance, R. L. Dewar, R. B. White, R. C. Grimm, J. Manickam, H. R. Strauss, J. L. Johnson, J. M. Greene, A. H. Glasser, P. K. Kaw, P. H. Rutherford, and E. J. Valeo, in *Eighth International Conference on Plasma Physics and Controlled Nuclear Fusion* (IAEA, Vienna, 1981), vol. 1, pp. 227–235, paper IAEA-CN-38/J-1.

[16] W. Park, E. D. Fredrickson, A. Janos, J. Manickam, and W. M. Tang, *Phys. Rev. Lett.* **75**, 1763 (1995).

[17] R. G. Kleva and P. N. Guzdar, *Phys. Rev. Lett.* **80**, 3081 (1998).

[18] S. C. Cowley and M. Artun, *Phys. Rep.* **283**, 185 (1997).

[19] O. A. Hurricane, B. H. Fong, and S. C. Cowley, *Phys. Plasmas* **4**, 3565 (1997).

[20] H. R. Wilson and S. C. Cowley, *Phys. Rev. Lett.* **92**, 175006 (2004).

[21] P. Zhu, C. C. Hegna, and C. R. Sovinec, *Phys. Plasmas* **13**, 102307 (2006).

[22] P. Zhu, C. C. Hegna, C. R. Sovinec, A. Bhattacharjee, and K. Germaschewski, *Phys. Plasmas* **14**, 055903 (2007).

[23] P. Zhu and C. C. Hegna, *Phys. Plasmas* **15**, 092306 (2008).

[24] A. Kirk, B. Koch, R. Scannell, H. R. Wilson, G. Counsell, J. Dowling, A. Herrmann, R. Martin, M. Walsh, and the MAST team, *Phys. Rev. Lett.* **96**, 185001 (2006).

[25] A. Kirk, G. F. Counsell, G. Cunningham, J. Dowling, M. Dunstan, H. Meyer, M.Price, S.Saarelma, R.Scannell, M.Walsh, H. R. Wilson, and the MAST team, *Plasma Phys. Control. Fusion* **49**, 1259 (2007).

[26] P. B. Snyder, H. R. Wilson, and X. Q. Xu, *Phys. Plasmas* **12**, 056115 (2005).

[27] C. R. Sovinec, D. C. Barnes, R. A. Bayliss, D. P. Brennan, E. D. Held, S. E. Kruger, A. Y. Pankin, D. D. Schnack, and the NIMROD Team, *J. Phys.: Conf. Ser.* **78**, 012070 (2007).

[28] J. W. Connor, R. J. Hastie, and J. B. Taylor, *Proc. R. Soc. Lond. A.* **365**, 1 (1979).

[29] D. Pfirsch and R. N. Sudan, *Phys. Fluids B* **5**, 2052 (1993).

[30] C. Sovinec, A. Glasser, D. Barnes, T. Gianakon, R. Nebel, S. Kruger, D. Schnack, S. Plimpton, A. Tarditi, M. Chu, and the NIMROD Team, *J. Comput.Phys.* **195**, 355 (2004).

[31] L. E. Zakharov and A. Pletzer, *Phys. Plasmas* **6**, 4693 (1999).

[32] P. Zhu, A. Bhattacharjee, and K. Germaschewski, *Phys. Rev. Lett.* **96**, 065001 (2006).

[33] B. H. Fong, S. C. Cowley, and O. A. Hurricane, *Phys. Rev. Lett.* **82**, 4651 (1999).